UNIVERSITEIT VAN PRETORIA
UNIVERSITY OF PRETORIA
YUNIBESITHI YA PRETORIA

CHAPTER 3

MODEL IDENTIFICATION

3.1 Literature Review

Hearns et al. [8] and Anbe et al. [9] consider the rolling process as multivariable with interaction between strip tensions and thickness and designed an H_∞ controller for the process. [8] and [9] tested their designs on a nonlinear model and a real plant respectively. Their designs were for the threading speed phase of rolling and for a multi stand mill in contrast to this work in which controllers were designed for the speed up phase of a reversing hot rolling mill. In their linear time invariant (LTI) rolling mill model Anbe et al. use tension stress instead of tension as a controlled and state variable. This is an effective way of approaching the control of tension stress because stress is of interest rather than only tension as it is done in this work. However it is also sufficient to use tension as controlled variable because deviations from the setup value of the strip cross section are only very small compared to the total cross section area.

Hearns et al. did their controller design later than Anbe et al. and showed that robust stability in the presence of a changing mill modulus is achievable while still obtaining high performance such as strip thickness accuracy, thereby bypassing the robustness/performance trade-off to an extent.

Pedersen et al. [21] also viewed the hot rolling process as multivariable for controller design purposes. In contrast to [8] and [9] Pedersen et al. investigated plate rolling and the focus mainly was on thickness control by means of a linear quadratic regulator (LQR).

UNIVERSITEIT VAN PRETORIA
UNIVERSITY OF PRETORIA
YUNIBESITHI YA PRETORIA

In the projects of [8] and [9] the process variables do not vary across the width of the strip. With regard to this aspect [8] and [9] differ from the work done in [12] and [21]. In [12], however, a Generalised Predictive Controller (GPC) was designed to work on a supervisory level. The control design methodology thus differs from [8], [9] and [21] in so far that a time-varying controller with no fixed structure was designed – it has no fixed structure because an optimization problem is solved at each time step. However similar to the other three projects Grimble et al. [12] did their design for a multivariable multi stand rolling process at threading speed, i.e. steady state. In particular the process variables selected for control in [12] are gauge, profile and temperature.

This shows that the work done in this dissertation most closely resembles that done in [9] but is different from it in the sense that it is done for control of a reversing mill on the speed up ramp.

3.2 Modeling Considerations

The available nonlinear model for the Steckel mill is not in a format that can directly be used for controller design purposes. Therefore an identification of a linear model from the nonlinear simulator was first performed.

For the variable classification of the linear model the outputs of interest are the centerline thickness of the strip and the strip tensions on either side of the roll gap. Hydraulic stroke set points on both sides of the mill frame and back and front coiler peripheral speeds become the choice for the manipulated variables as intervention into the process is possible through these variables. In Laplace transfer function format the LTI model is then

$$\begin{bmatrix} \delta h_2(s) \\ \delta T_1(s) \\ \delta T_2(s) \end{bmatrix} = \begin{bmatrix} g_{11}(s) & g_{12}(s) & g_{13}(s) \\ g_{21}(s) & g_{22}(s) & g_{23}(s) \\ g_{31}(s) & g_{32}(s) & g_{33}(s) \end{bmatrix} \begin{bmatrix} \delta x_{sp}(s) \\ \delta v_{bc}(s) \\ \delta v_{fc}(s) \end{bmatrix}, \tag{3.1}$$

or in standard transfer function model notation,

$$y(s) = G(s)u(s) \tag{3.2}$$

where

$$y(s) = [\delta h_2(s) \quad \delta T_1(s) \quad \delta T_2(s)]^T :$$

the controlled variable vector,

$$u(s) = [\delta x_{sp}(s) \quad \delta v_{bc}(s) \quad \delta v_{fc}(s)]^T :$$

the manipulated variable vector.

A system identification technique (SID) is applied to the simulator of the process in order to get an LTI estimate of the nonlinear model for controller design. As the simulator consists of several sub models of the process (see Fig. 3.1), of which the TM and the RGM are implicitly related to each other, a linearization of the nonlinear model via an algebraic method would possibly not be suitable to reflect such a relationship satisfactorily [24]. The use of the Matlab System Identification toolbox [25] was therefore chosen to obtain the linear model. Fig. 3.1 is derived from the input/output relationships given in Table 3.1.

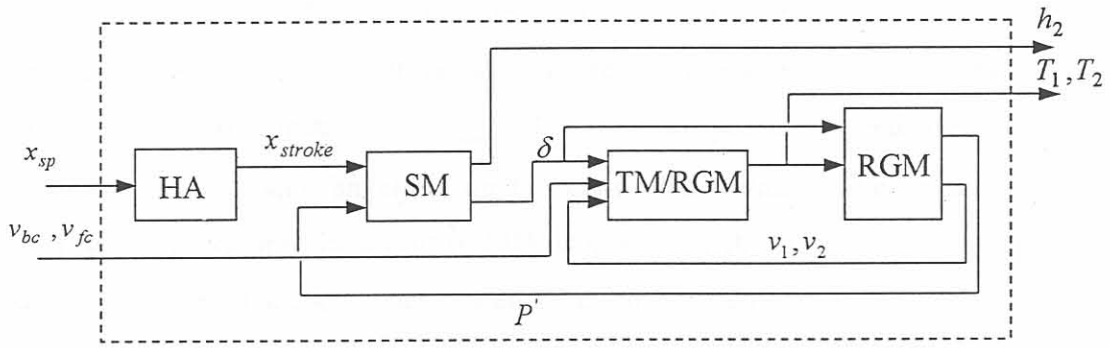

Figure 3.1: Block diagram of rolling process with I/O information.

Table 3.1: Inputs and outputs for process models.

Model	Inputs	Outputs
Hydraulic actuator (HA)	x_{sp}	x_{stroke}
Stand model (SM)	P', x_{stroke}	δ, h_2
Roll gap model (RGM)	δ, T_1, T_2	P', v_1, v_2
Tension model (TM)	v_1, v_2, v_{bc}, v_{fc}	T_1, T_2

With respect to the linear model as in Eq. 3.1 it is suitable to use a least squares method and solve for the best values of parameters of a transfer function that fit the time domain

UNIVERSITEIT VAN PRETORIA
UNIVERSITY OF PRETORIA
YUNIBESITHI YA PRETORIA

data. These parameters are the coefficients of difference equation models for the process in which the current output is a function of previous values of the output and present and past values of the input. This is a linear relationship in the time domain, which can easily be converted into Laplace domain transfer function models [26] as desired for Eq. 3.1. By means of the Matlab System Identification toolbox ARX (Auto Regression with external input) linear transfer functions could be identified as elements of the MIMO plant in Eq. 3.1.

In the case of the least squares method any form of inputs can be used to generate data for SID but it was suggested in [4] to use steps with the main reason being the absence of a plant bandwidth, which is necessary to design a PRBS input signal.

In [13] the potential economic benefit for a rolling process of operating the mill optimally on the speed up and slow down phases of rolling was investigated. The results of these findings motivated the decision to choose an operating point and point of linearization during the acceleration phase of the mill. At the point of linearization the main mill drive speed was forced constant at $v_{main} = 3.5$ ms^{-1} to prevent speed deviations during acceleration from having an effect on the controlled outputs. The validity of the LTI model, which is obtained by means of SID, is limited by the size of the coiler speed steps, discussed in the next section. These speed steps can be used as limits because for the speed range of validity only the difference between the coilers peripheral speed and the main drive speed matters, such that the valid speed range is $v_{main} = 3.5 \pm 0.2$ ms^{-1}.

Steps were used as inputs to the simulator and the results used to identify the linear transfer functions between inputs and outputs. Because the reasoning behind the design of step tests in [4] were found to be plausible, the same steps were applied to the simulator in this work. The only difference to [4] lies in the values that were used for the initial states of the upper roll pack. In this work the initial states were given the first nonzero values, which are obtained during the steady state development of the exit gauge, whereas in [4] zero initial states were assumed. The reason for the use of nonzero initial states was to achieve a bumpless start up of the simulations.

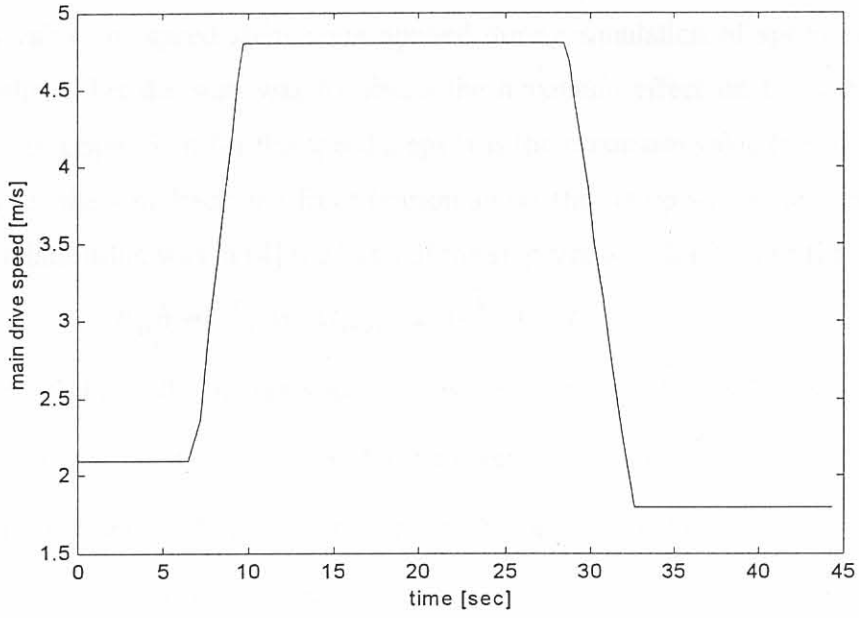

Figure 3.2: Main drive speed during pass 3 of the rolling process.

3.3 Step Tests

The steps are applied to the simulator at the point where the main mill drive speed is forced constant during the speed up phase of the mill.

3.3.1 Hydraulic Stroke Set Points, δx_{sp}

In [4] it is shown that the exit gauge changes even when no inputs are changed. A hydraulic stroke of 1mm was not exceeded in [12] when a supervisory GPC (Generalized Predictive Control)- controller was used to regulate the rolling process. Based on this information the same size of a step was suggested by [4]. The same author found that a 1 mm step is below the 2 mm bound of the step size, at which the strength limit of the mill frame is reached.

Because of the steady state development of the exit gauge, the effective dynamic behaviour of the mill due to a step in hydraulic stroke set point is the difference between the response of a step in hydraulic stroke and the response of a steady state simulation.

3.3.2 Speed Steps, $\delta v_{bc}, \delta v_{fc}$

Maximum values of speed steps were applied during simulation of speed step tests. The thought behind this decision was to obtain the maximum effect on the centerline output gauge [4]. An upper limit for the speed steps was the maximum value (i.e. a stress value of 200 MPa) for the strip back and front tension above the set up stress value of 8 MPa. The following relationship was in [4] the basis of the step size and duration of the step:

$$E_{ss} h_i w L_{rgcf}^{-1} \Delta v_c \Delta t_{step} = 2 \cdot 10^8 h_i w - T_{i\ setup} \tag{3.3}$$

where $i \in [1,2]$ for roll gap entrance and exit respectively. E_{ss} is Young's modulus for stainless steel, w the strip width, h the strip thickness and L_{rgcf} the length of the strip between the roll gap and the coiler furnace. A speed step $\Delta v_c = \pm 0.2$ ms^{-1} and a step duration $\Delta t_{step} = 60 \cdot 10^{-3}$ s was used.

3.4 Identification

In this section the inputs applied to the simulator as well as the corresponding output responses are given in the form of graphs and are discussed heuristically.

Three different linear models have been identified. In this work they will be called the first, the second and the third linear model and are given and discussed in sections 3.4.1, 3.4.2 and 3.4.3 respectively. Tab. 3.2 gives an overview of the differences between these three LTI models with respect to four criteria listed in the first column of the table.

Because of long simulation times involved (in excess of 6 days for 10 s of process time on a Pentium III, 533 MHz) to produce data for system identification purposes, the amount of data was sufficient to fit models but insufficient for a validation data range. For some of the transfer functions the quality of fit is however given in terms of auto-correlation plots of the error signal of the model output and also in terms of cross-correlation plots of the error signal and the input of a model.

Table 3.2: Differences between the three identified linear models.

Linear Model	1	2	3
Is TM part of simulator ?	SID data for all transfer functions, except for $g_{11}(s)$, were generated with the TM being part of the simulator.	SID data for all transfer functions were generated with the TM being part of the simulator.	SID data for all transfer functions were generated with the TM being part of the simulator.
Are non zero off-diagonal transfer functions present ?	Non zero off-diagonal transfer functions are: $g_{21}(s), g_{31}(s), g_{23}(s)$ and $g_{32}(s)$.	This linear model is decoupled, i.e. no non zero off-diagonal transfer functions.	All off-diagonal transfer functions are non zero.
Is gauge meter compensation incorporated in simulator ?	No	Yes	Yes
Are tensions controlled in an inner loop ?	No	Yes	Yes

3.4.1 First Linear Model

3.4.1.1 The Transfer Function $g_{11}(s)$

The transfer function $g_{11}(s)$ relates hydraulic stroke as input to centerline exit gauge as output, i.e. it relates exit gauge to that manipulated variable by which it is influenced most directly. Because constant exit gauge is a measure of strip quality, $g_{11}(s)$ represents the most important transfer function of the process. Its model was fitted as

$$g_{11}(s) = \frac{-8.2551 \cdot 10^{-2}}{s + 1.9942 \cdot 10^{-1}} e^{-2.5 \cdot 10^{-2} s} = \frac{-4.1936 \cdot 10^{-1}}{5.0145 s + 1} e^{-2.5 \cdot 10^{-2} s} . \quad (3.4)$$

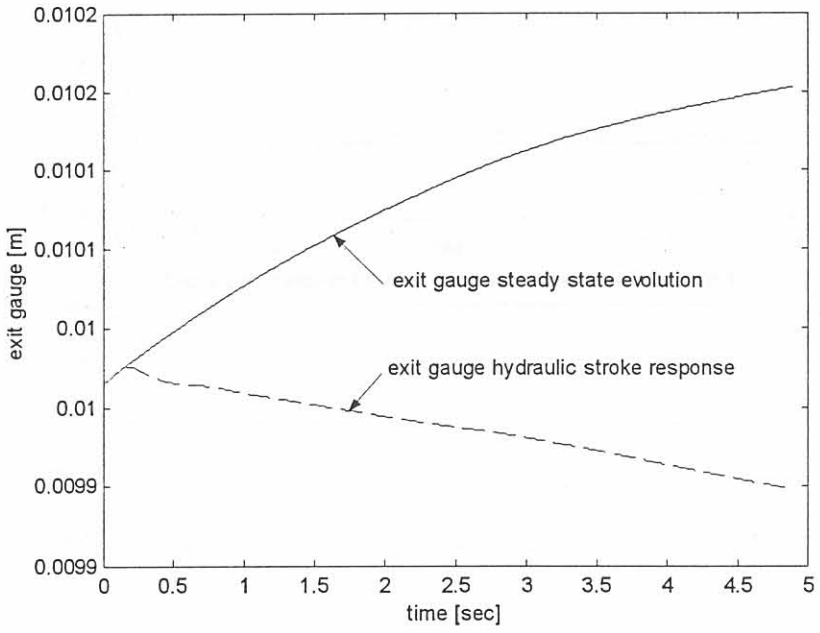

Figure 3.3: Steady state evolution of exit gauge and trend of exit gauge due to a hydraulic actuator stroke of 1 mm.

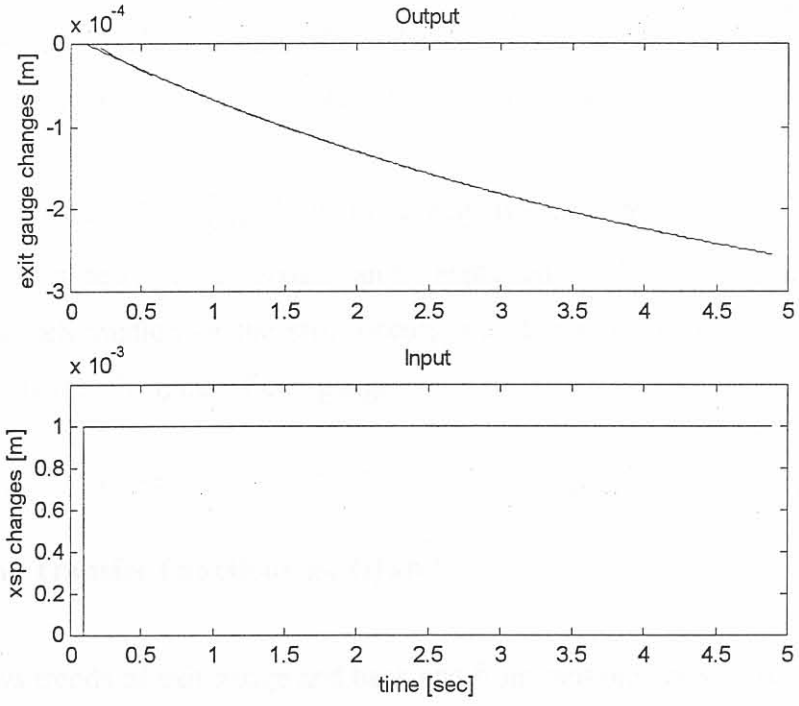

Figure 3.4: I/O data for the identification of $g_{11}(s)$ in the first linear model. (for outputs: solid: model output, dashed: measured output).

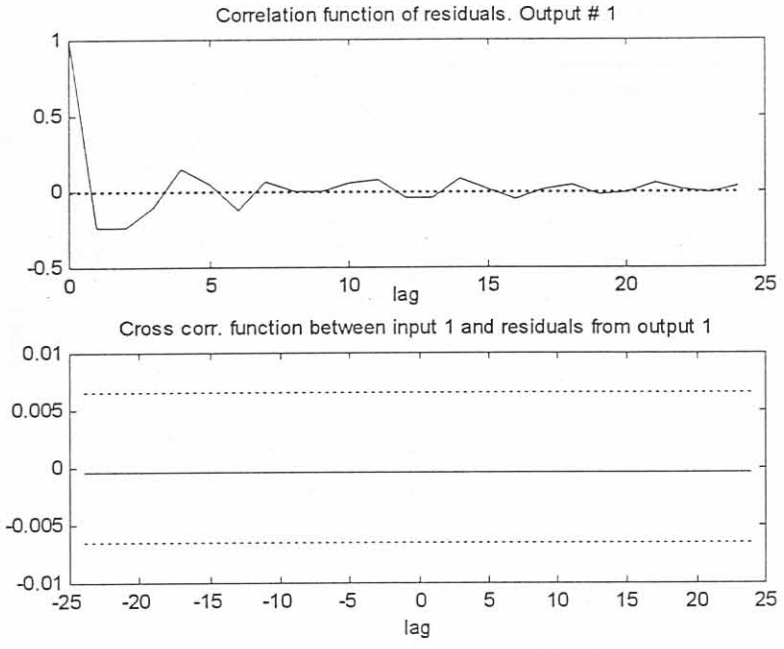

Figure 3.5: Correlation and cross correlation plots of the fitted model for $g_{11}(s)$. The dotted lines indicate the 99 % confidence level.

The output data for this transfer function as given in Fig. 3.4 was obtained by subtracting the steady state evolution of the exit thickness in Fig. 3.3 from the exit thickness data which resulted from the application of a hydraulic actuator stroke (also in Fig. 3.3). This is done in order to obtain the dynamic effect due to actuator stroke set point change.

As shown with Fig. 3.4, $g_{11}(s)$ is of a negative first order form with a delay of milliseconds. This delay of exit gauge can be explained by elastic mill stretch taking place before plastic deformation of the strip occurs, i.e. it is due to the time constant of mill stretch being shorter than that of exit gauge.

3.4.1.2 The Transfer Functions $g_{21}(s)$ and $g_{31}(s)$

Fig. 3.6 shows trends of exit gauge and back and front tensions for steady state, i.e. no step input, with the tensions allowed to vary uncontrolled. It can be seen from Fig. 3.6 that as exit gauge increases, i.e. as the roll gap opens, tensions also increase.

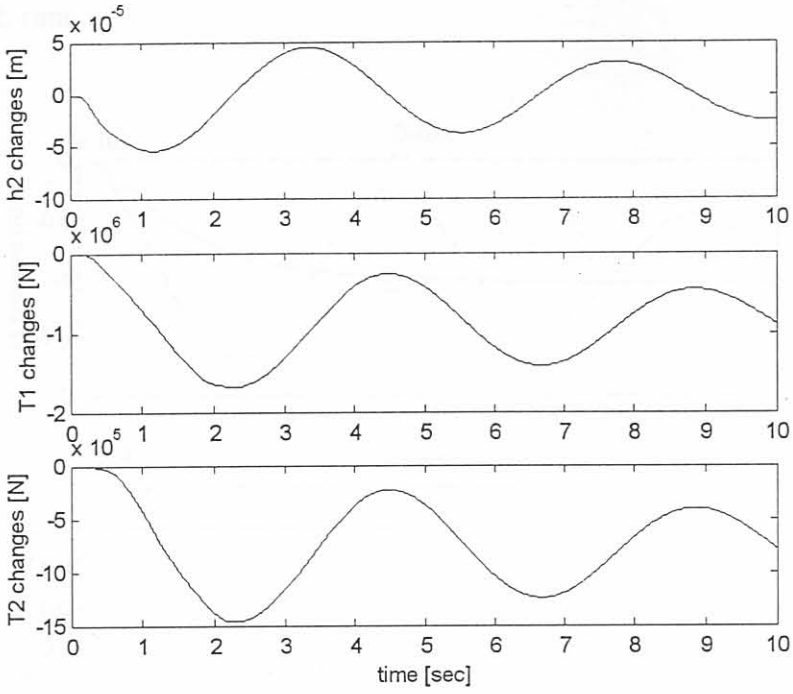

Figure 3.6: Trends of h_2, T_1 and T_2 with tensions uncontrolled and without application of steps on inputs.

The increase in front tension is caused by a decrease in exit speed, v_2, of the strip at the roll gap. v_2 decreases because the material flow, $h_1 v_1$ or $h_2 v_2$, through the roll gap changes in such a way that more material is allowed to travel through the roll gap, i.e. increase of v_1, but not enough to let v_2 increase, because h_2 increases in such a way that v_2 decreases in order for mass flow continuity to hold through the roll gap, i.e.

$$h_1 v_1 = h_2 v_2 \tag{3.5}$$

Tensions then increase to such an extent that they cause material deformation, which results in a thinner strip and therefore decrease of exit thickness as can be seen from Fig. 3.6.

Figures 3.7 and 3.9 show the input/output data that was used for the identification of the transfer functions $g_{21}(s)$ and $g_{31}(s)$ respectively. $g_{21}(s)$ and $g_{31}(s)$ relate hydraulic stroke set point change as input to back and front tension changes respectively as outputs. The output data for $g_{21}(s)$ and $g_{31}(s)$ was obtained by a subtraction similar as was done

for $g_{11}(s)$ in the previous section. It can be seen that the amplitude of tension oscillations decreases with time.

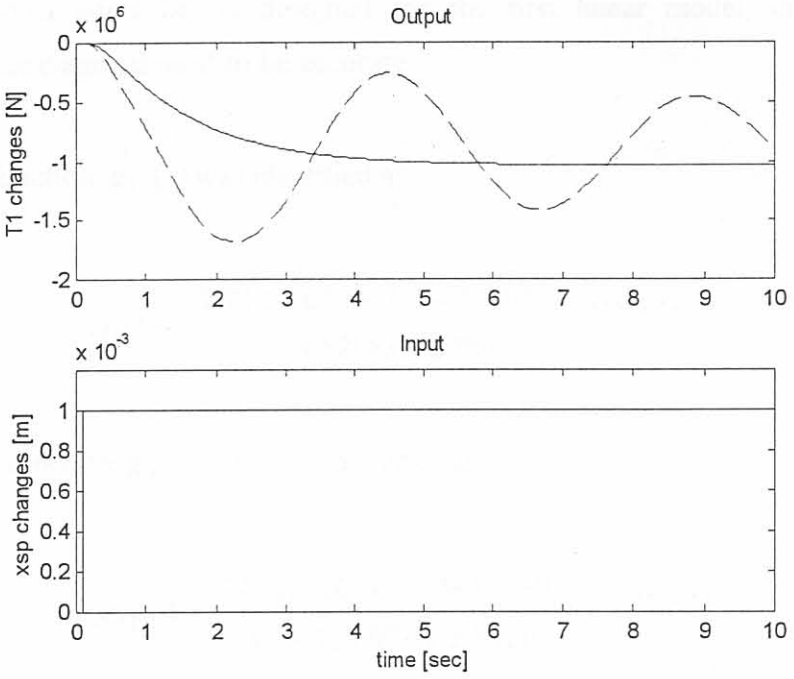

Figure 3.7: I/O data for the identification of $g_{21}(s)$ in the first linear model. (for outputs: solid: model output, dashed: measured output).

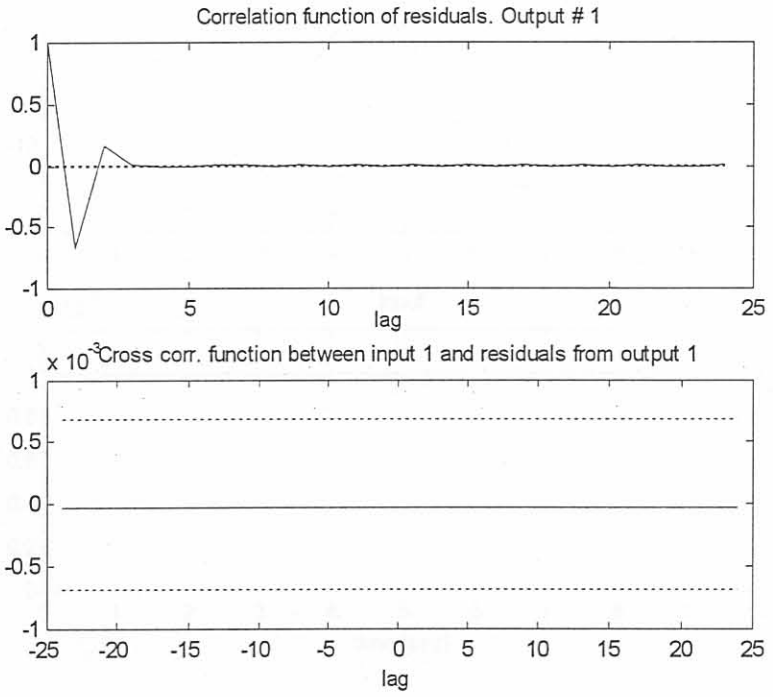

Figure 3.8: Correlation and cross correlation plots of the fitted model for $g_{21}(s)$. The dotted lines indicate the 99 % confidence level.

During identification of $g_{21}(s)$ and $g_{31}(s)$ it was found that high order models improved the accuracy of the fit. High order models are however impractical for controller design. Since a diagonal controller is designed for the first linear model, only the transfer functions on the diagonal need to be accurate.

The transfer function $g_{21}(s)$ was identified as

$$g_{21}(s) = \frac{7.712 \cdot 10^4 s - 3.0847 \cdot 10^9}{s^2 + 4.5298s + 2.966} \cdot e^{-7.25 \cdot 10^{-2} s}, \tag{3.6}$$

while transfer function $g_{31}(s)$ has been obtained as

$$g_{31}(s) = \frac{6.4215 \cdot 10^4 s - 2.5685 \cdot 10^9}{s^2 + 4.2697s + 2.8926} \cdot e^{-7.75 \cdot 10^{-2} s}. \tag{3.7}$$

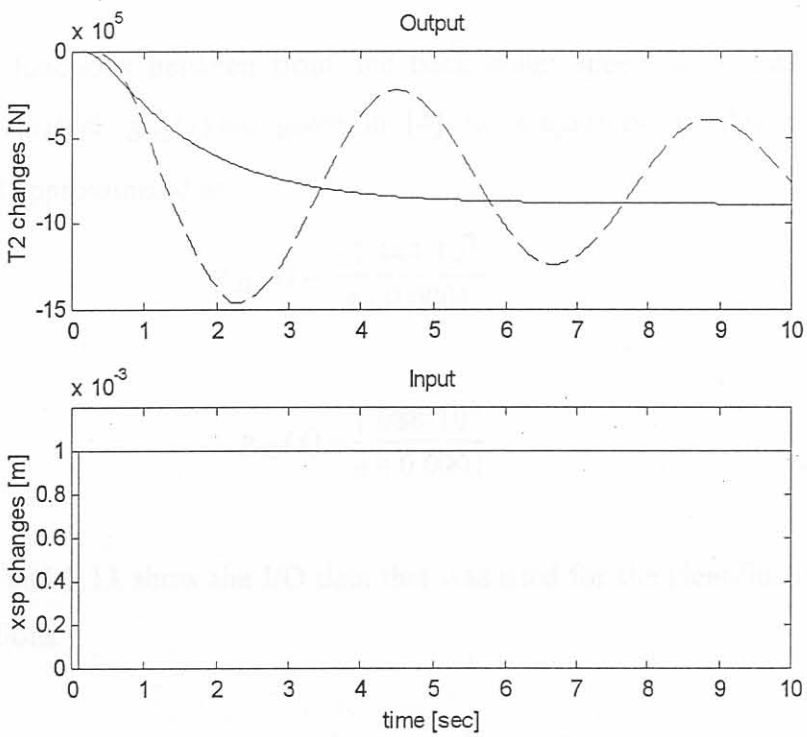

Figure 3.9: I/O data for the identification of $g_{31}(s)$ in the first linear model. (for outputs: solid: model output, dashed: measured output).

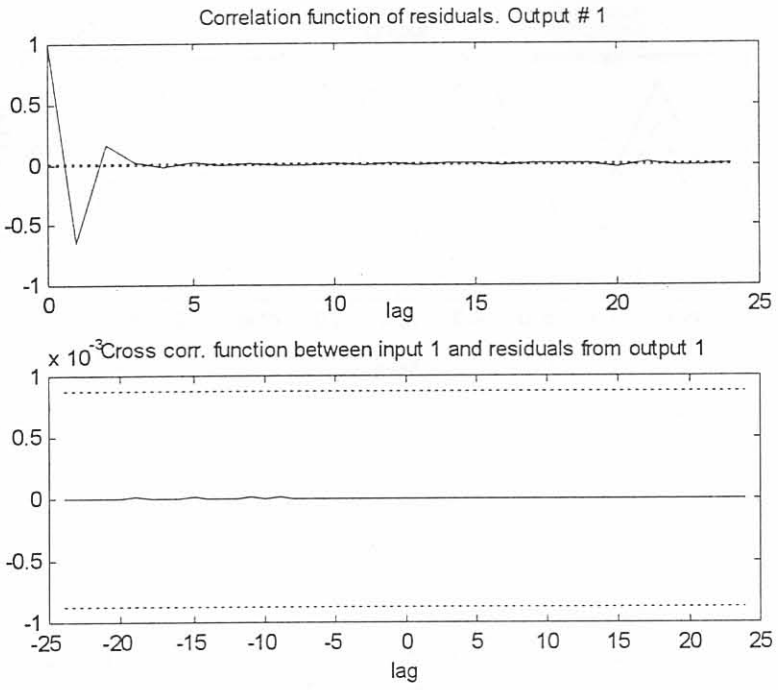

Figure 3.10: Correlation and cross correlation plot of the fitted model for $g_{31}(s)$ in the first linear model. The dotted lines indicate the 99% confidence level.

3.4.1.3 The Transfer Functions $g_{22}(s)$ and $g_{33}(s)$

The transfer functions between front and back coiler speed steps and front and back tensions, $g_{33}(s)$ and $g_{22}(s)$ are given in [4] as integrators. In this work they were identified and approximated as

$$g_{22}(s) = \frac{-1.444 \cdot 10^8}{s + 0.0001} \tag{3.8}$$

and

$$g_{33}(s) = \frac{1.088 \cdot 10^8}{s + 0.0001}. \tag{3.9}$$

Figures 3.11 and 3.13 show the I/O data that was used for the identification of these two transfer functions.

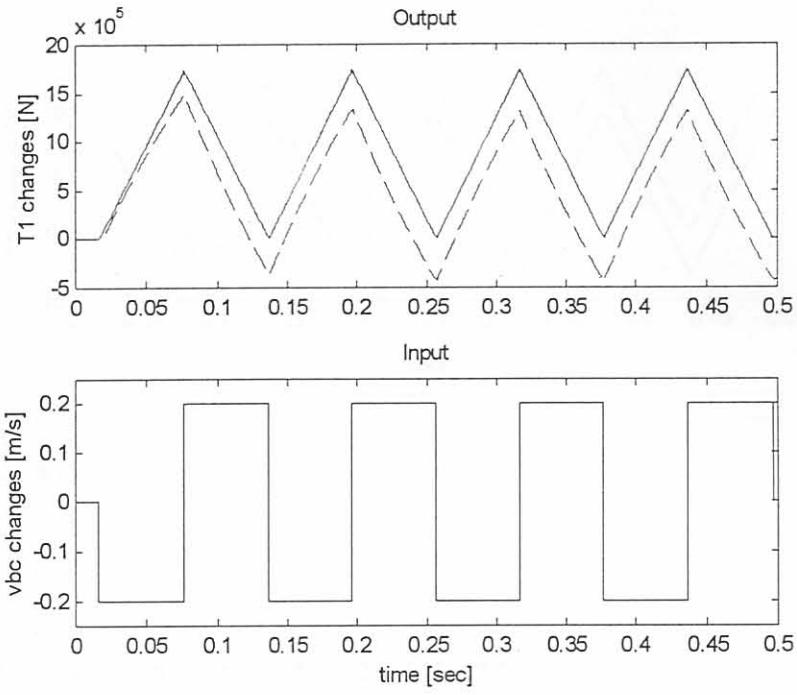

Figure 3.11: I/O data for the identification of $g_{22}(s)$ in the first linear model. (for outputs: solid: model output, dashed: measured output).

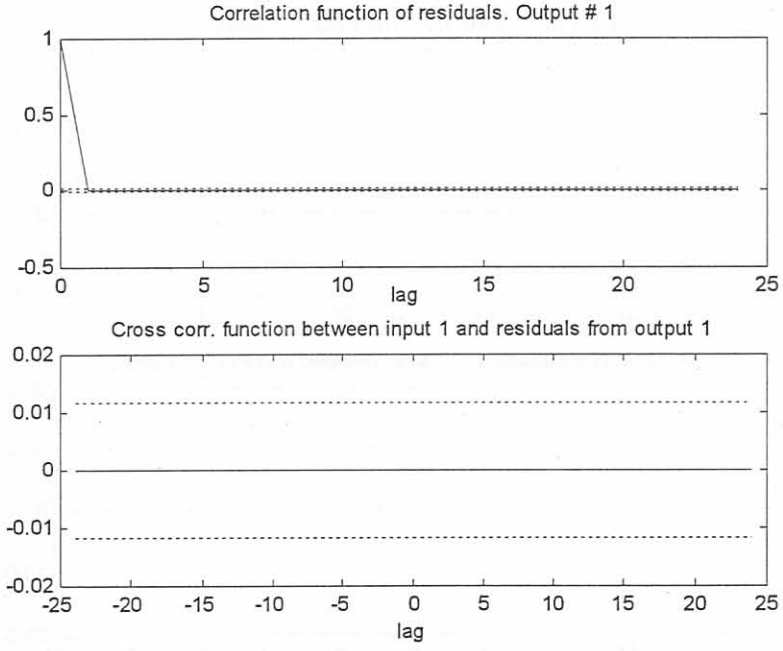

Figure 3.12: Correlation and cross correlation plot of the fitted model for $g_{22}(s)$ in the first linear model. The dotted lines indicate the 99% confidence level.

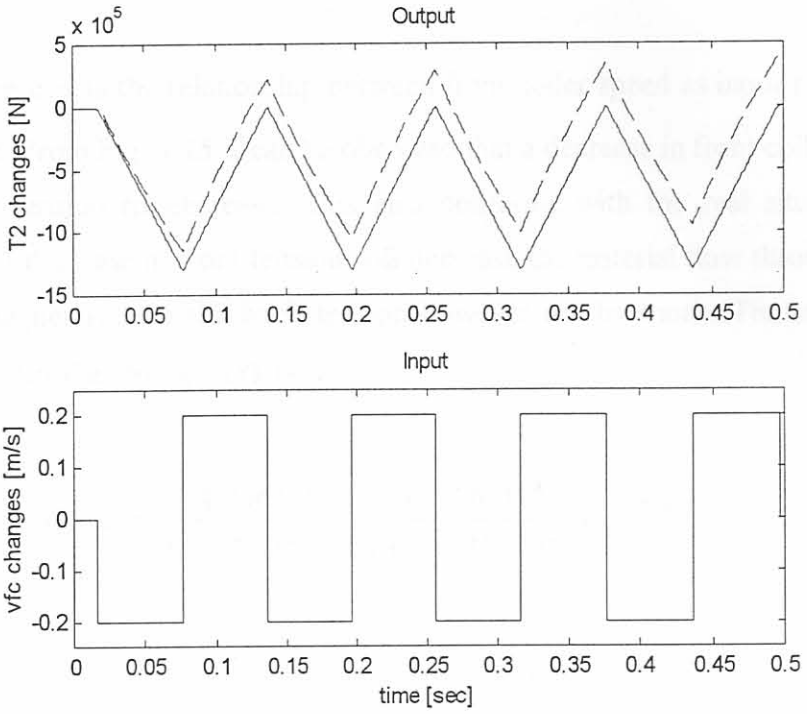

Figure 3.13: I/O data for the identification of $g_{33}(s)$ in the first linear model. (for outputs: solid: model output, dashed: measured output).

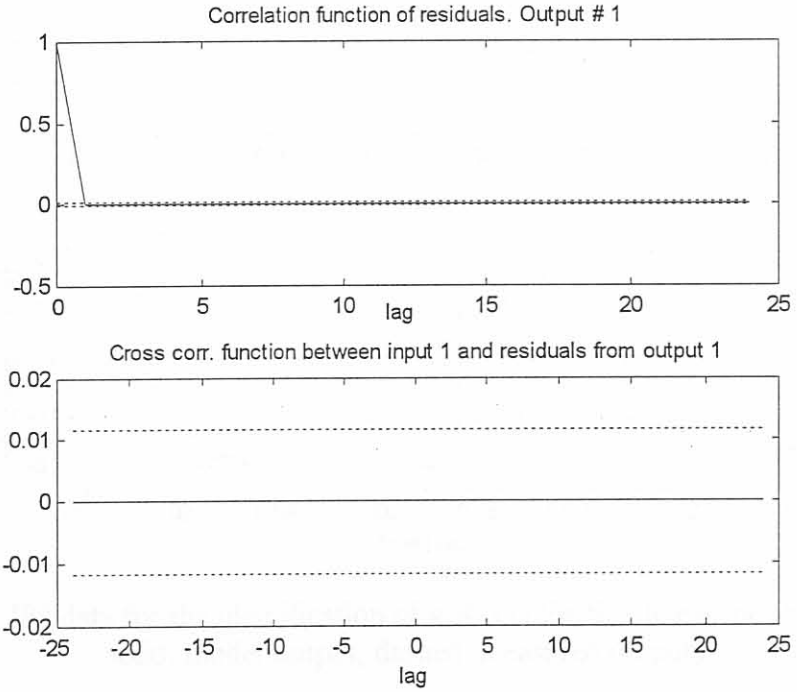

Figure 3.14: Correlation and cross correlation plot of the fitted model for $g_{33}(s)$ in the first linear model. The dotted lines indicate the 99% confidence level.

3.4.1.4 The Transfer Functions $g_{23}(s)$ and $g_{32}(s)$

$g_{23}(s)$ represents the relationship between front coiler speed as input and back tension as output. From Fig. 3.15 it can be observed that a decrease in front coiler speed causes the back tension to decrease. This also conforms with the real situation since the associated decrease in front tension will decrease the material flow through the roll gap and consequently also the back tension however not by much. The transfer function that was identified for $g_{23}(s)$ is

$$g_{23}(s) = \frac{-1.2461 \cdot 10^4 s + 6.1196 \cdot 10^8}{s^2 + 4.0453 \cdot 10 s + 4.0318 \cdot 10^2} \cdot e^{-2.15 \cdot 10^{-2} s} \quad (3.10)$$

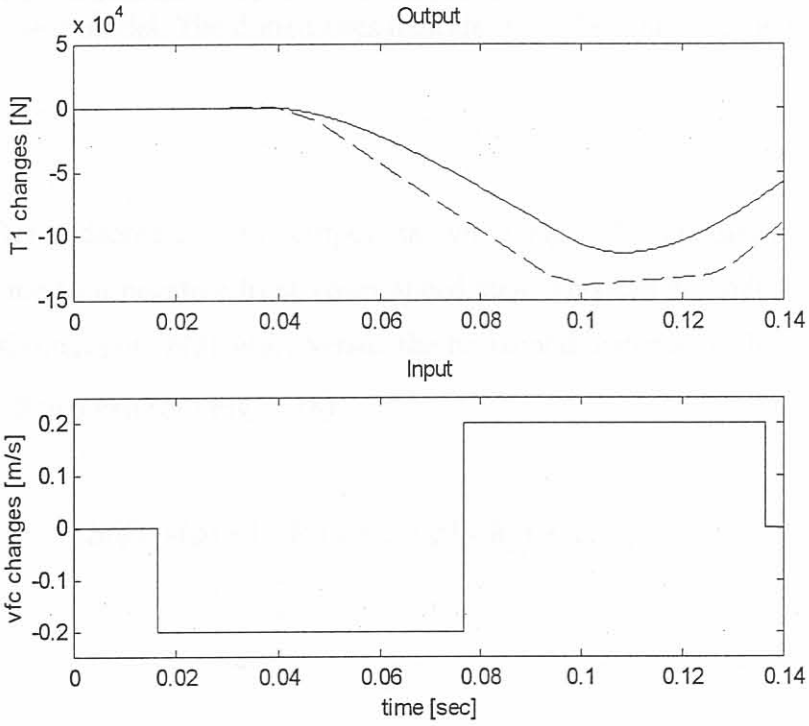

Figure 3.15: I/O data for the identification of $g_{23}(s)$ in the first linear model (for outputs: solid: model output, dashed: measured output).

UNIVERSITEIT VAN PRETORIA
UNIVERSITY OF PRETORIA
YUNIBESITHI YA PRETORIA

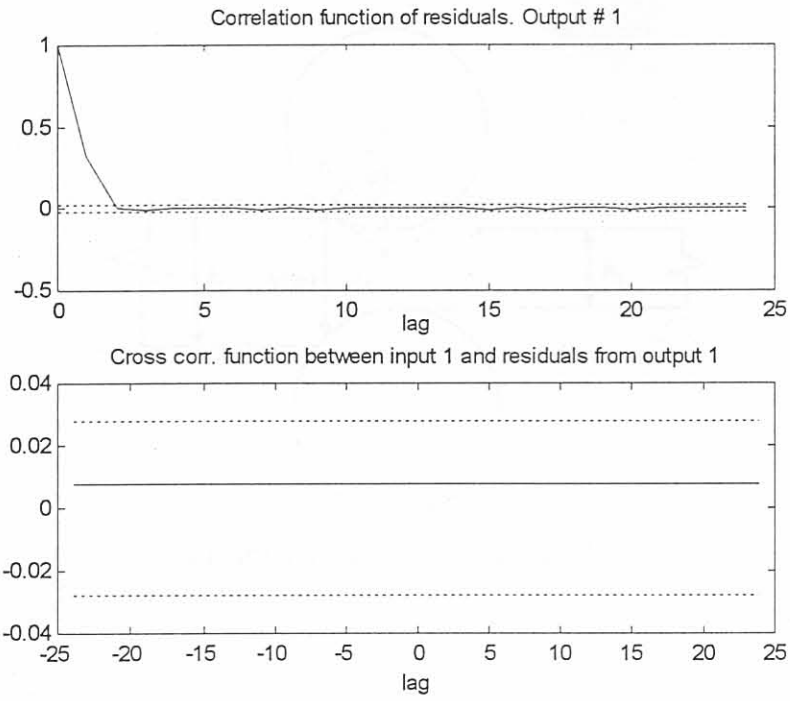

Figure 3.16: Correlation and cross correlation plot of the fitted model for $g_{23}(s)$ in the first linear model. The dotted lines indicate the 99% confidence level.

A flat part after a decrease of the output, shown in Fig. 3.15, appears like saturation of back tension due to a negative front coiler speed step. This can be understood by using a graph of the throughput, $h(\phi)\cdot v(\phi)$, versus the horizontal distance of the neutral point, at ϕ, from the roll gap exit (see Fig. 3.18).

$$h(\phi)\cdot v(\phi)=\left(2R'(1-\cos\phi)+h_2\right)v_r\cos\phi \quad , \tag{3.11}$$

where

v_r: peripheral speed of work rollers and

$R'\sin\phi$: horizontal distance of neutral point from roll gap exit.

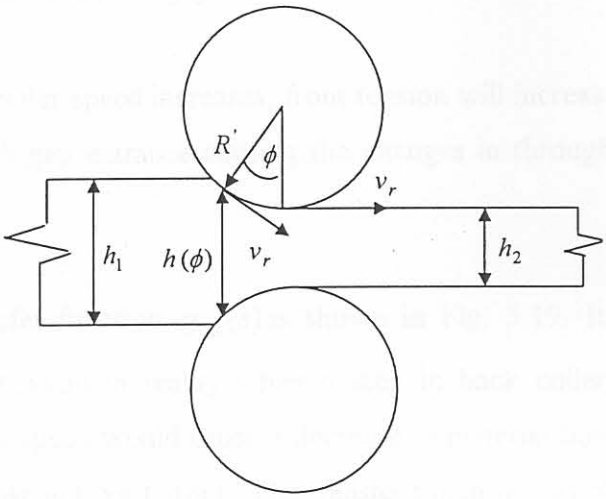

Figure 3.17: Roll gap geometry.

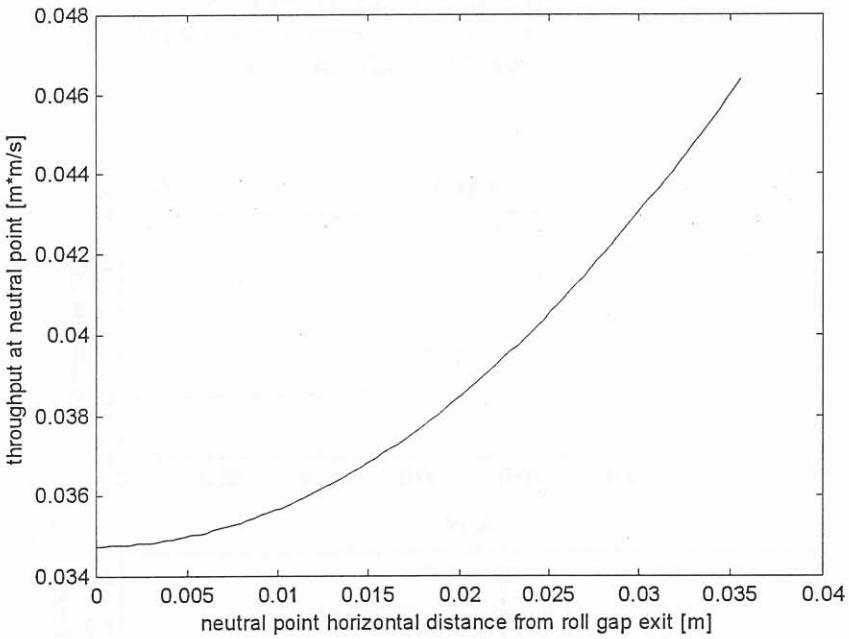

Figure 3.18: Throughput versus horizontal position of the neutral point from the roll gap exit.

When front tension decreases, which happens for a negative step in front coiler speed, a surplus of back tension, will cause the neutral point to shift towards the exit of the roll gap [24] decreasing the throughput , $h(\phi)\cdot v(\phi)$, and causing the back tension to decrease only until it saturates. The saturation occurs because the changes in throughput are only negligible, when the neutral point is close to the roll gap exit as Fig. 3.18 shows. This

UNIVERSITEIT VAN PRETORIA
UNIVERSITY OF PRETORIA
YUNIBESITHI YA PRETORIA

explains why nonlinear saturation behaviour of back tension appears as a result of the neutral point being close to the roll gap exit.

However when front coiler speed increases, front tension will increase and shift the neutral point closer to the roll gap entrance causing the changes in throughput to become more pronounced.

I/O data for the transfer function $g_{32}(s)$ is shown in Fig. 3.19. It reflects what would happen to the front tension in reality when a step in back coiler speed is applied. A decrease in back coiler speed would cause a decrease in material flow through the roll gap and therefore an increase in front tension. The transfer function was obtained as

$$g_{32}(s) = \frac{2.3159 \cdot 10^4 s - 9.0907 \cdot 10^8}{s^2 + 43.528s + 92.486} \cdot e^{-2.0 \cdot 10^{-2} s} \quad (3.12)$$

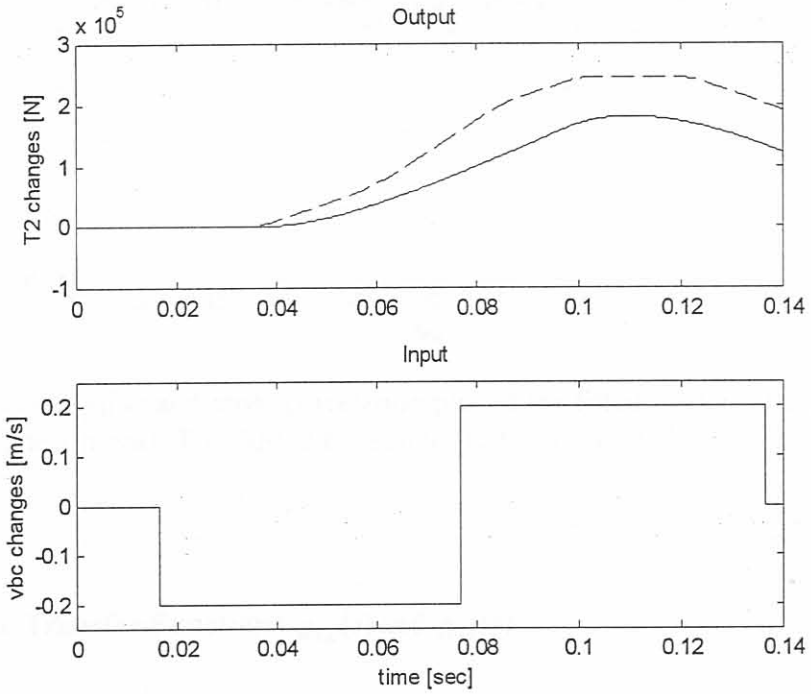

Figure 3.19: I/O data for the identification of $g_{32}(s)$ in the first linear model (for outputs: solid: model output, dashed: measured output).

The saturation phenomena of front tension due to a negative step in back coiler speed shown in Fig. 3.19 can be explained in a similar way as the saturation of back tension in Fig. 3.15.

The cross correlation plots are an indication of the linear independence between the input and the residual of the real and estimated model. The offsets of the cross correlation functions in figures 3.16 and 3.20 could therefore be caused by the attempt made to fit linear models on I/O data which shows a nonlinear saturation effect in figures 3.15 and 3.19.

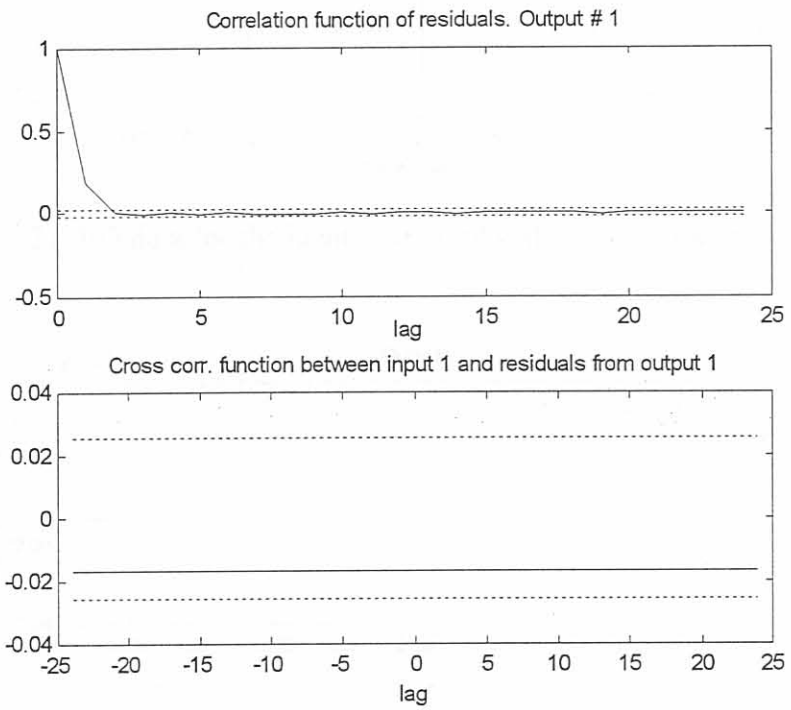

Figure 3.20: Correlation and cross correlation plot of the fitted model for $g_{32}(s)$ in the first linear model. The dotted lines indicate the 99% confidence level.

3.4.1.5 The Transfer Functions $g_{12}(s)$ and $g_{13}(s)$

The influence of the step in back coiler speed given in Fig. 3.21 on exit gauge is by a factor of approximately 60 smaller than the influence of a step in hydraulic actuator stroke set point given in Fig. 3.4. Therefore the influence of back coiler speed on exit gauge was neglected and the transfer function was chosen as

$$g_{12}(s) = 0. \tag{3.13}$$

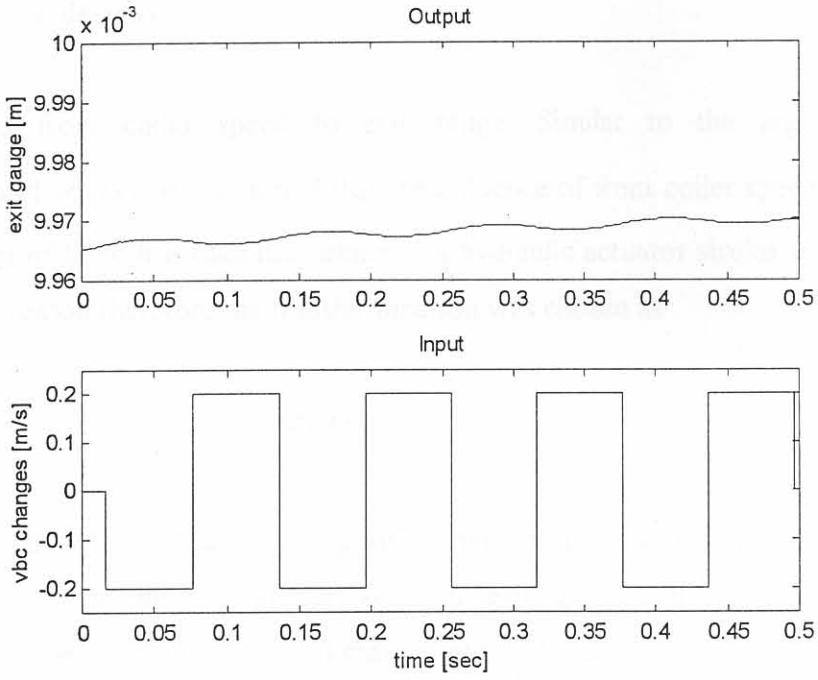

Figure 3.21: I/O data for the identification of $g_{12}(s)$ in the first linear model.

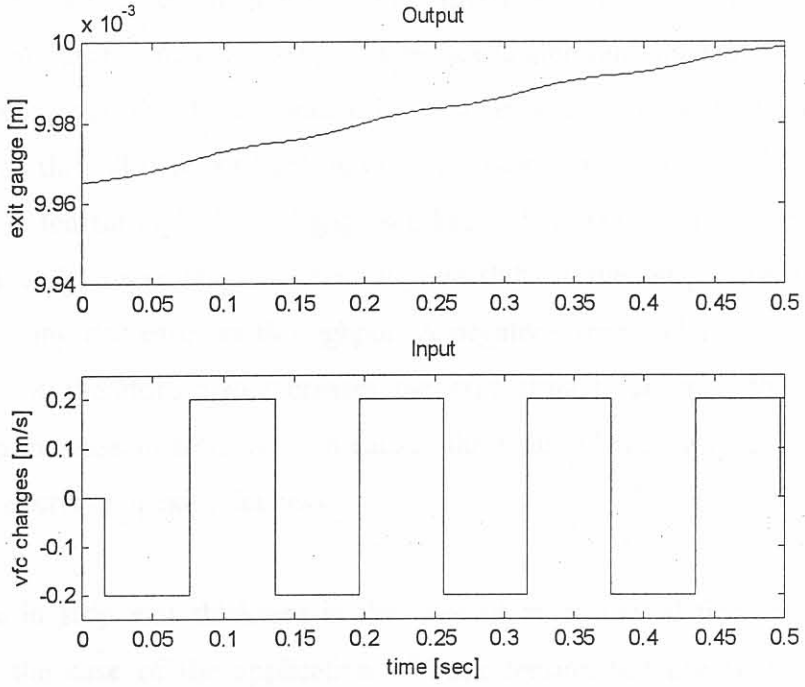

Figure 3.22: I/O data for the identification of $g_{13}(s)$ in the first linear model.

Fig. 3.21 is showing the I/O data for $g_{12}(s)$. From this figure one can see that for a decrease in back coiler speed and therefore an increase in back tension the trend of exit gauge is changed into a decreasing trend. This makes sense from a practical point of view

UNIVERSITEIT VAN PRETORIA
UNIVERSITY OF PRETORIA
YUNIBESITHI YA PRETORIA

since tension helps with the deformation, i.e. thickness reduction, of the material, causing the exit gauge to decrease.

$g_{13}(s)$ relates front coiler speed to exit gauge. Similar to the argument for the identification of $g_{12}(s)$, it was found that the influence of front coiler speed on exit gauge is by an order of $1 \cdot 10^2$ less than the influence of hydraulic actuator stroke set point change. For a similar reason therefore the transfer function was chosen as

$$g_{13}(s) = 0 \ . \tag{3.14}$$

One can see from Fig. 3.22 that a positive step in front coiler speed causes a slight decreasing trend in the second derivative of exit gauge which reflects a plausible relationship between front coiler speed changes and exit gauge.

If the I/O data of $g_{12}(s)$ is compared with that of $g_{13}(s)$, the question arises why exit gauge in general increases when front coiler speed steps are applied while it shows an almost constant general trend when back coiler speed steps are applied. The reason for the decreasing exit gauge due to a negative back coiler speed step is that the neutral point moves towards the roll gap exit because of an increased back tension, which indicates that less material is fed through the roll gap (see Fig. 3.18) resulting in a thinner strip. With negative back coiler speed steps the neutral point shifts to the left part of the curve in Fig. 3.18, thus causing decreases in throughput. A negative front coiler speed step decreases front tension. It therefore also increases the separating force such that exit thickness increases. An increase in front tension causes the required rolling force to decrease and with it also a decrease in exit thickness.

The decrease in strip exit thickness in the case of an increased front tension is not as severe as in the case of the application of back tension because with increased front tension the neutral point shifts towards the roll gap entrance resulting in more throughput. One therefore has more throughput together with a surplus of rolling force which cancel each other to an extent.

Back tension is also known to be twice as effective as front tension in decreasing the separating force between the work rolls [20] thus decreasing the strip exit thickness more severely when it is applied.

3.4.2 Second Linear Model

3.4.2.1 The Transfer Function $g_{11}(s)$

Fig. 3.23 shows the input and output data used to identify $g_{11}(s)$. The output represents the exit gauge steady state evolution subtracted from the exit gauge trend during an input as shown by the bottom curve of Fig. 3.23.

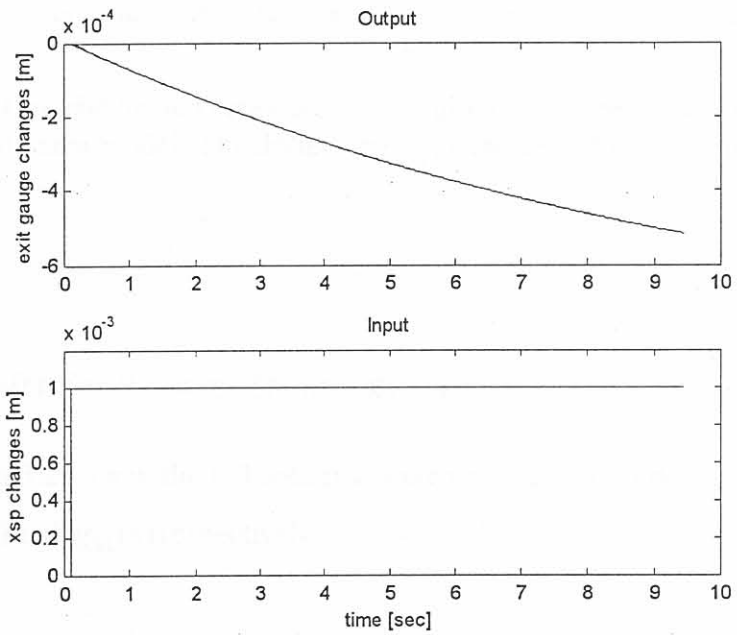

Figure 3.23: I/O data for the identification of $g_{11}(s)$ in the second linear model. (for outputs: solid: model output, dashed: measured output).

From Fig.3.23 and also from the steady state gain of $g_{11}(s)$ it can be registered that although the gauge meter compensation was present in the simulation, the input step of 1mm is not completely converted into change of exit gauge but only to about 87 %. This can be attributed to the fact that tensions were not regulated at perfectly constant values. The transfer function obtained for $g_{11}(s)$ is

$$g_{11}(s) = \frac{-8.3334 \cdot 10^{-2}}{s + 9.5039 \cdot 10^{-2}} \cdot e^{-2.5 \cdot 10^{-2} s} = \frac{-0.8768}{10.52s + 1} \cdot e^{-2.5 \cdot 10^{-2} s}. \qquad (3.15)$$

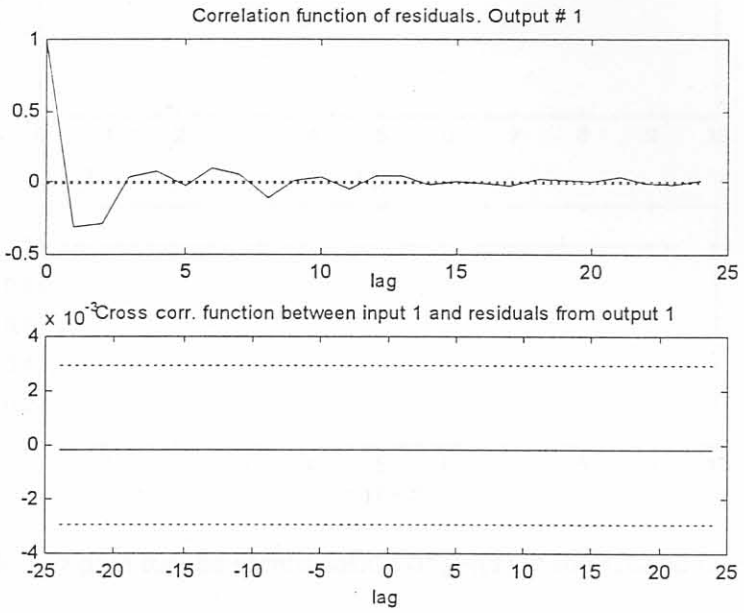

Figure 3.24: Correlation and cross correlation plot of the fitted model for $g_{11}(s)$ in the second linear model. The dotted lines indicate the 99% confidence level.

3.4.2.2 Transfer Functions $g_{21}(s)$ and $g_{31}(s)$

Figures 3.25 and 3.26 show the I/O data that were used to make a decision on the transfer functions $g_{21}(s)$ and $g_{31}(s)$ respectively.

Because of the close to constant outputs of $g_{21}(s)$ and $g_{31}(s)$ it was decided to use

$$g_{21}(s) = 0 \qquad (3.16)$$

and

$$g_{31}(s) = 0. \qquad (3.17)$$

Constant output data for $g_{21}(s)$ and $g_{31}(s)$ were also obtained by subtracting the steady state simulations of the tensions from the tension trends obtained during a hydraulic stroke step test as done for the identification of $g_{11}(s)$.

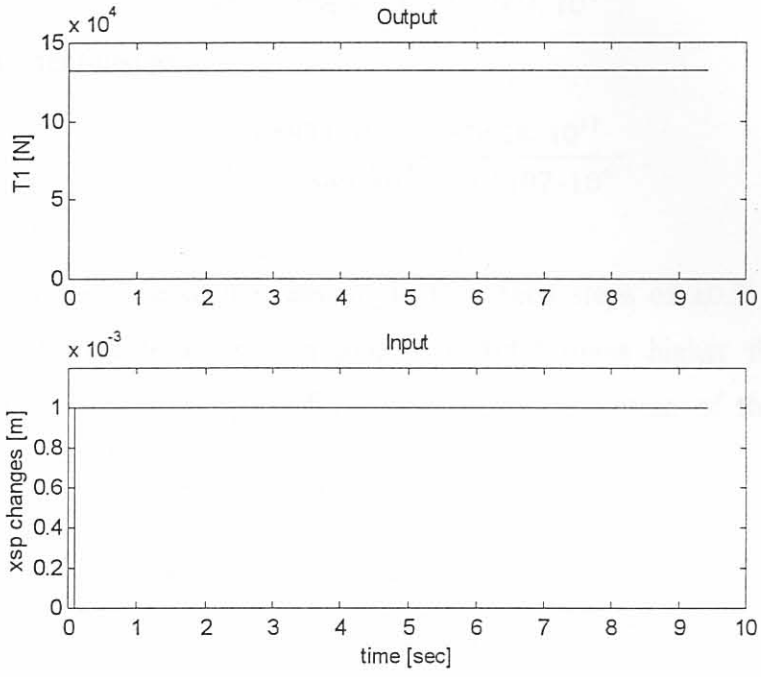

Figure 3.25: I/O data for the identification of $g_{21}(s)$ in the second linear model.

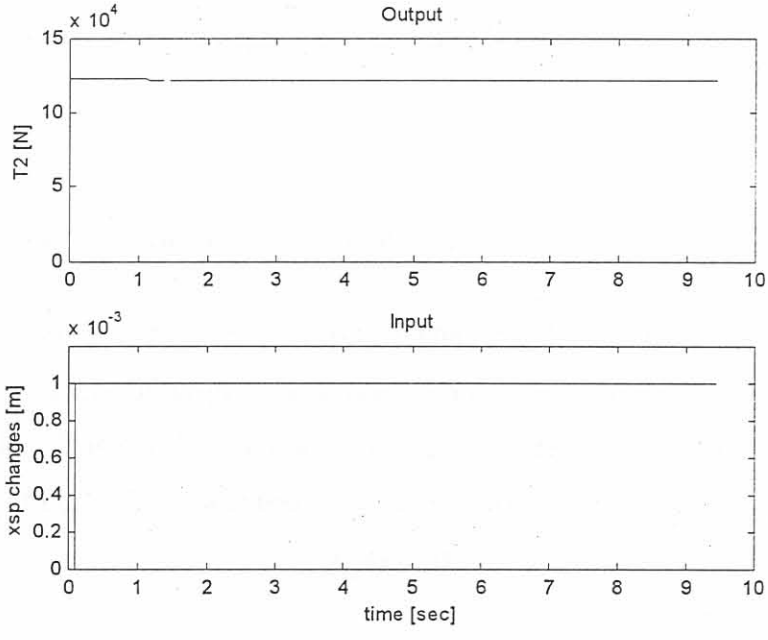

Figure 3.26: I/O data for the identification of $g_{31}(s)$ in the second linear model.

3.4.2.3 Transfer Functions $g_{22}(s)$ and $g_{33}(s)$

Figures 3.27 and 3.29 show the I/O data used for the identification of $g_{22}(s)$ and $g_{33}(s)$.

$g_{22}(s)$ was identified as

UNIVERSITEIT VAN PRETORIA
UNIVERSITY OF PRETORIA
YUNIBESITHI YA PRETORIA

$$g_{22}(s) = \frac{-6.9002 \cdot 10^6 s - 1.3594 \cdot 10^{12}}{s^2 + 9.0963 \cdot 10^3 s + 5.071 \cdot 10^6} \tag{3.18}$$

and $g_{33}(s)$ was identified as

$$g_{33}(s) = \frac{-4.5934 \cdot 10^6 s + 9.0628 \cdot 10^{11}}{s^2 + 8.1846 \cdot 10^3 s + 5.5107 \cdot 10^6} \tag{3.19}$$

The higher order response of the tensions to the speed steps of ±0.2 m/s is due to the control applied to the tensions at a frequency 1000 times higher than the sampling frequency of the outer main loop of the simulator. The design of these controllers is discussed in section 5.3.

In figures 3.28 and 3.30 auto and cross correlation plots are given for the models fitted for $g_{22}(s)$ and $g_{33}(s)$ respectively. The correlation present in the auto correlation plots of figures 3.28 and 3.30, indicate that the model structures for $g_{22}(s)$ and $g_{33}(s)$ can still be improved. It was found that their structural fit improved when models of a higher order than given above for $g_{22}(s)$ and $g_{33}(s)$ were identified. The cross correlation present for positive lags in figures 3.28 and 3.30 are a consequence of the improvable model structures.

3.4.2.4 Transfer Functions $g_{12}(s)$ and $g_{13}(s)$

The changes of exit gauge in response to step changes of ±0.2 m/s of the coiler speeds are more than two orders of magnitude smaller than in its response to a step of 1 mm in hydraulic stroke. This can be seen when comparing the output data of figures 3.31 and 3.33 with that of Fig. 3.23. It was therefore decided to use

$$g_{12}(s) = 0 \tag{3.20}$$

and

$$g_{13}(s) = 0 \tag{3.21}$$

for the second linear model of the nonlinear plant.

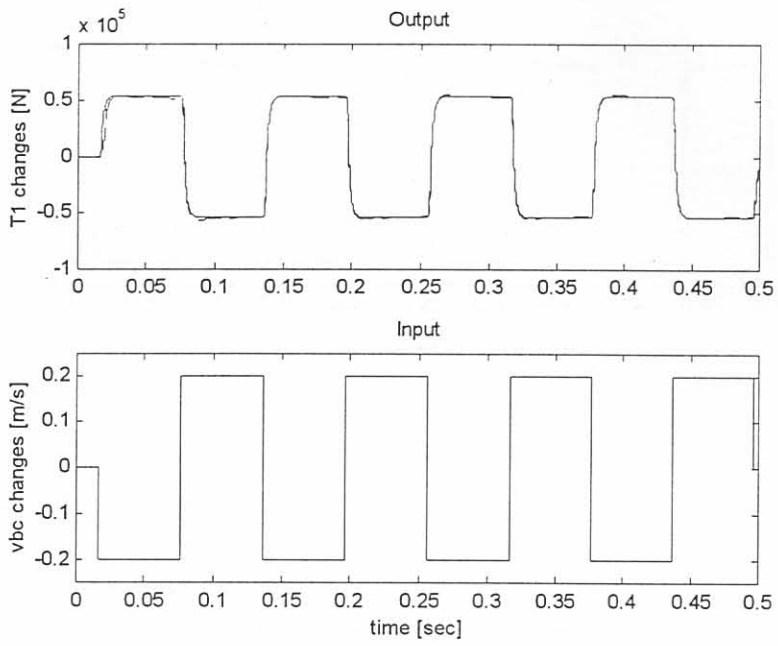

Figure 3.27: I/O data for the identification of $g_{22}(s)$ in the second linear model. (for outputs: solid: model output, dashed: measured output).

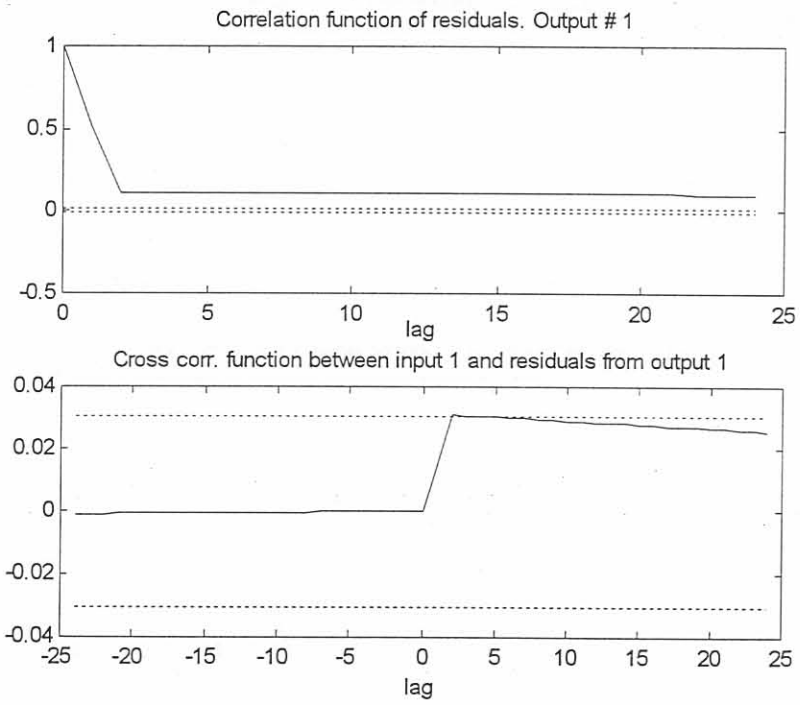

Figure 3.28: Correlation and cross correlation plot of the fitted model for $g_{22}(s)$ in the second linear model. The dotted lines indicate the 99% confidence level.

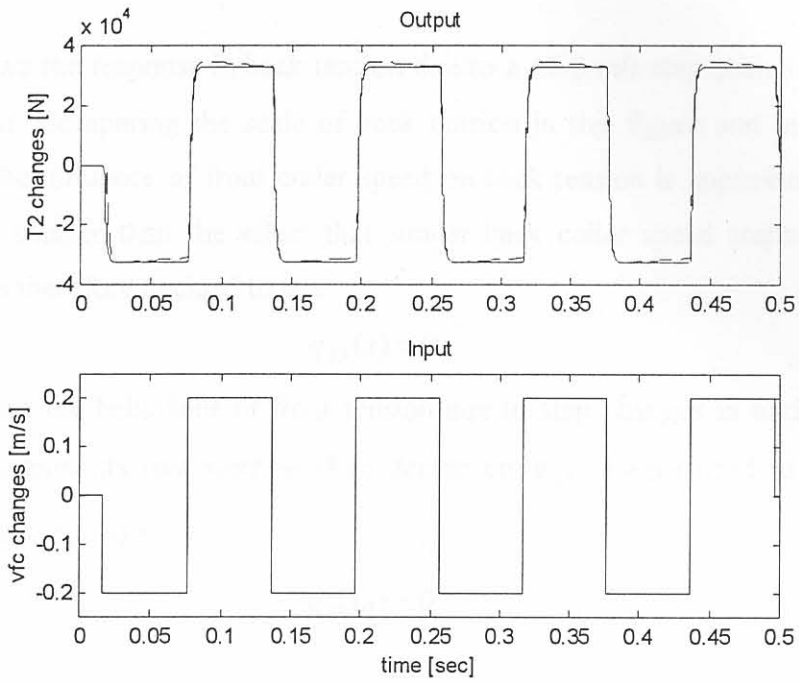

Figure 3.29: I/O data for the identification of $g_{33}(s)$ in the second linear model. (for outputs: solid: model output, dashed: measured output).

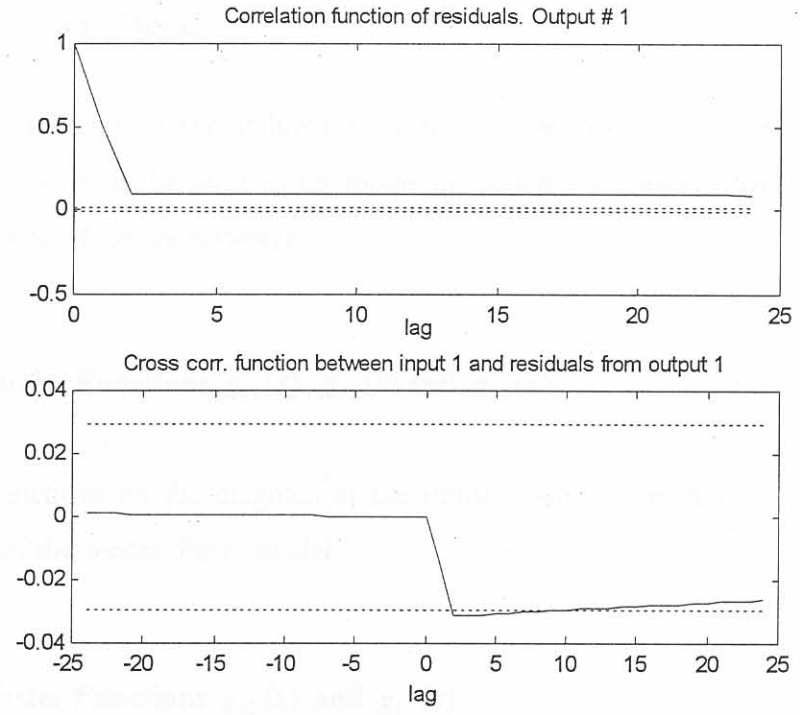

Figure 3.30: Correlation and cross correlation plot of the fitted model for $g_{33}(s)$ in the second linear model. The dotted lines indicate the 99% confidence level.

UNIVERSITEIT VAN PRETORIA
UNIVERSITY OF PRETORIA
YUNIBESITHI YA PRETORIA

3.4.2.5 Transfer Functions $g_{23}(s)$ and $g_{32}(s)$

Fig. 3.37 shows the response in back tension due to a ±0.2 m/s step change in front coiler speed as input. Comparing the scale of back tension in this figure and in Fig. 3.27 one realizes that the influence of front coiler speed on back tension is approximately 5 orders of magnitude smaller than the effect that similar back coiler speed steps have on back tension. It was therefore decided to use

$$g_{23}(s) = 0 \ . \tag{3.22}$$

Fig. 3.35 shows the behaviour of front tension due to step changes in back coiler speed. Here similar arguments that were used to decide on $g_{23}(s)$ were used to determine the transfer function $g_{32}(s)$ as

$$g_{32}(s) = 0 \tag{3.23}$$

for the second linear model of the nonlinear plant.

3.4.3 Third Linear Model

In an attempt to capture the influences of the interactions a third linear model was identified. This model is the same as the model in section 3.4.2 except for the off-diagonal transfer functions, which are non-zero.

3.4.3.1 Transfer Functions $g_{11}(s), g_{22}(s)$ and $g_{33}(s)$

The transfer functions on the diagonal of the transfer function matrix in Eq. 3.1 are the same as those of the second linear model.

3.4.3.2 Transfer Functions $g_{12}(s)$ and $g_{13}(s)$

In figures 3.31 and 3.33, exit gauge shows integrator behaviour in response to coiler speed steps. As it was seen in figures 3.27 and 3.29 the response of the tensions to the same speed steps is almost proportional, i.e. the tensions respond with steps (see figures 3.21 and 3.22). It makes sense that the response of exit gauge to a step change in back and front

coiler speeds is a ramp such as in figures 3.31 and 3.33 when compared to the exit gauge response due to the same inputs in the first linear model (see figures 3.21 and 3.22). The relationship between tensions and exit gauge can thus be approached as integrators.

The transfer function $g_{12}(s)$ has been identified as

$$g_{12}(s) = \frac{1.342 \cdot 10^{-5}}{s + 0.01}, \tag{3.24}$$

while the transfer function $g_{13}(s)$ was estimated as

$$g_{13}(s) = \frac{-7.73 \cdot 10^{-6}}{s + 0.01} \cdot e^{-3.57 \cdot 10^{-3} s}. \tag{3.25}$$

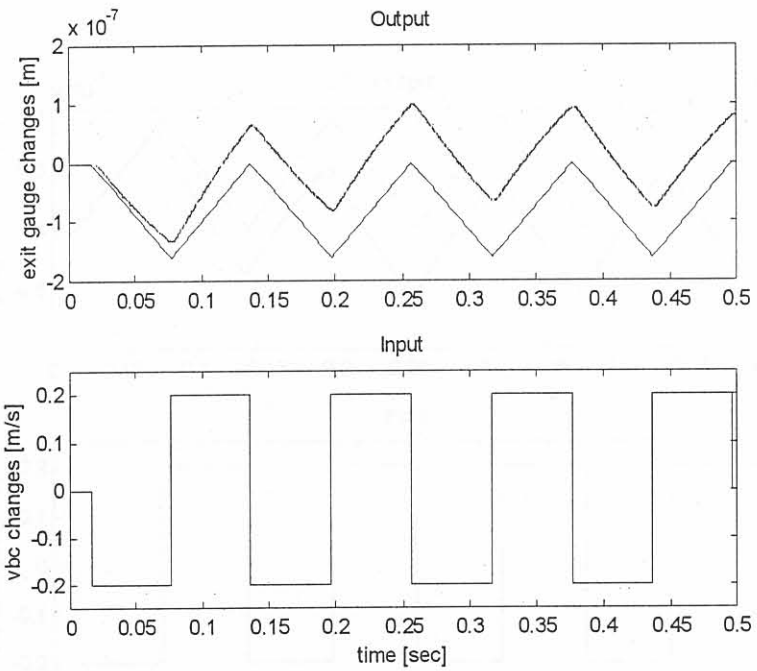

Figure 3.31: I/O data for the identification of $g_{12}(s)$ in the third linear model(for output: upper curve: measured output, lower curve: model output).

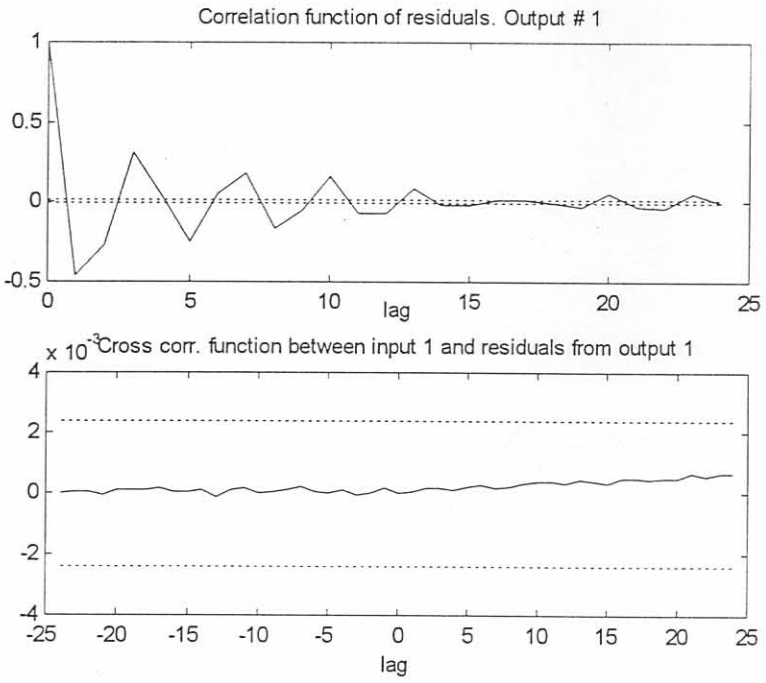

Figure 3.32: Correlation and cross correlation plot of the fitted model for $g_{12}(s)$ in the third linear model. The dotted lines indicate the 99% confidence level.

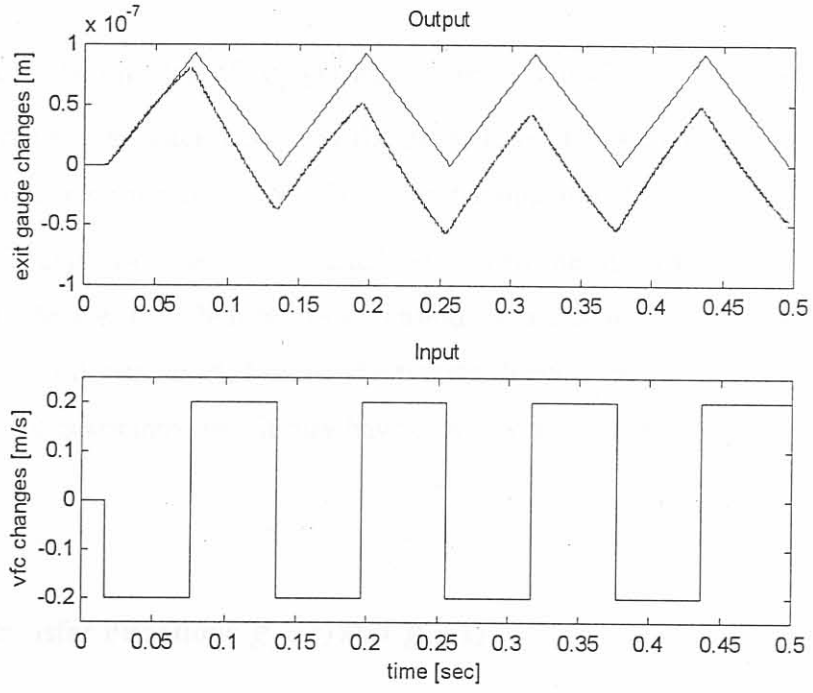

Figure 3.33: I/O data for the identification of $g_{13}(s)$ in the third linear model (for output: upper curve: model output, lower curve: measured output).

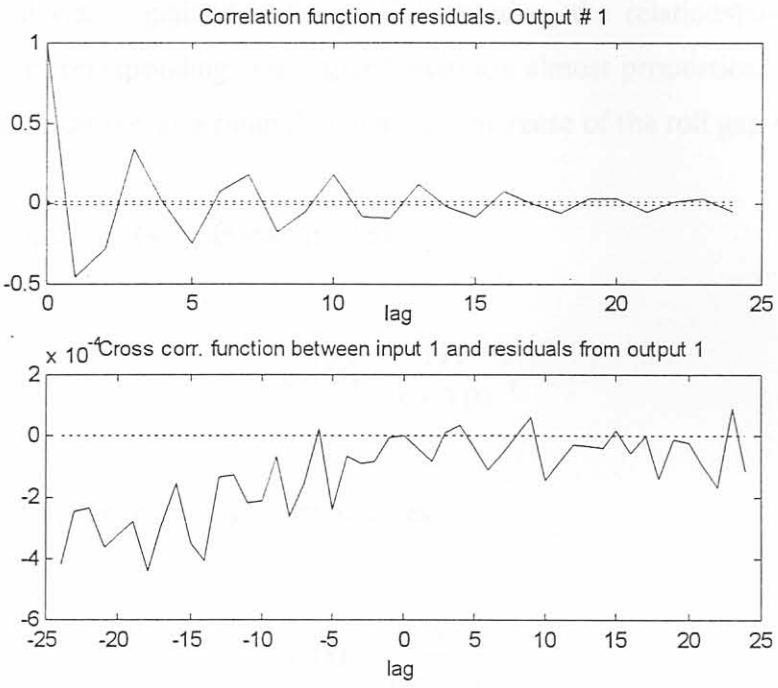

Figure 3.34: Correlation and cross correlation plot of the fitted model for $g_{13}(s)$ in the third linear model. The dotted lines indicate the 99% confidence level.

The cross correlation plot of $g_{13}(s)$ mainly shows correlation for negative lags, which means that output feedback occurs in the estimation of this transfer function. This could improve by changing the structure of the transfer function. The delay in $g_{13}(s)$ is only in the order of milliseconds and was added since with the application of front tension exit gauge must change first before back tension is affected. As an initial step towards controller design it was decided to use the transfer function as given in Eq. 3.25 since from its parameters it is assumed that it may have only a weak influence on exit gauge.

3.4.3.3 Transfer Functions $g_{32}(s)$ and $g_{23}(s)$

Fig. 3.35 shows the response of front tension to back coiler speed steps. For a negative back coiler speed step and thus increasing back tension the surplus of rolling force will cause the roll gap to become smaller and therefore deliver a thinner strip at a higher speed in order to maintain the throughput. This causes the front tension to drop. Because the exit gauge responds to back coiler speed steps and therefore to the back tension steps as a

UNIVERSITEIT VAN PRETORIA
UNIVERSITY OF PRETORIA
YUNIBESITHI YA PRETORIA

ramp, the roll gap exit speed will also change as a ramp in order to maintain the throughput. As it was explained in the previous section, the relationships between strip tensions and their corresponding coiler speed steps are almost proportional. Therefore the front tension will decrease as a ramp due to a ramp increase of the roll gap exit speed.

The transfer function $g_{32}(s)$ was identified as

$$g_{32}(s) = \frac{191}{s + 0.01}, \tag{3.26}$$

and the transfer function $g_{23}(s)$ was estimated as

$$g_{23}(s) = \frac{-452.1}{s + 0.01} \cdot e^{-3.57 \cdot 10^{-3} s}. \tag{3.27}$$

A delay in the order of milliseconds was incorporated in this transfer function because of the dead time involved for the exit gauge to change due to a change in front tension. This change of exit gauge is then registered in a change in back tension. For example, if the front tension decreases as a negative step because of a step decrease in front coiler speed the exit gauge would increase as a ramp (see section 3.4.3.2) causing more material to pass through thereby increasing the entry speed as a ramp. This would then result in a proportional, i.e. also ramp increase of back tension.

Pertaining the auto correlation plots of the transfer function estimation for $g_{23}(s)$ (see Fig. 3.38), similar comments as those made about the auto correlation plots for $g_{13}(s)$ (see Fig. 3.34) in section 3.4.3.2 apply.

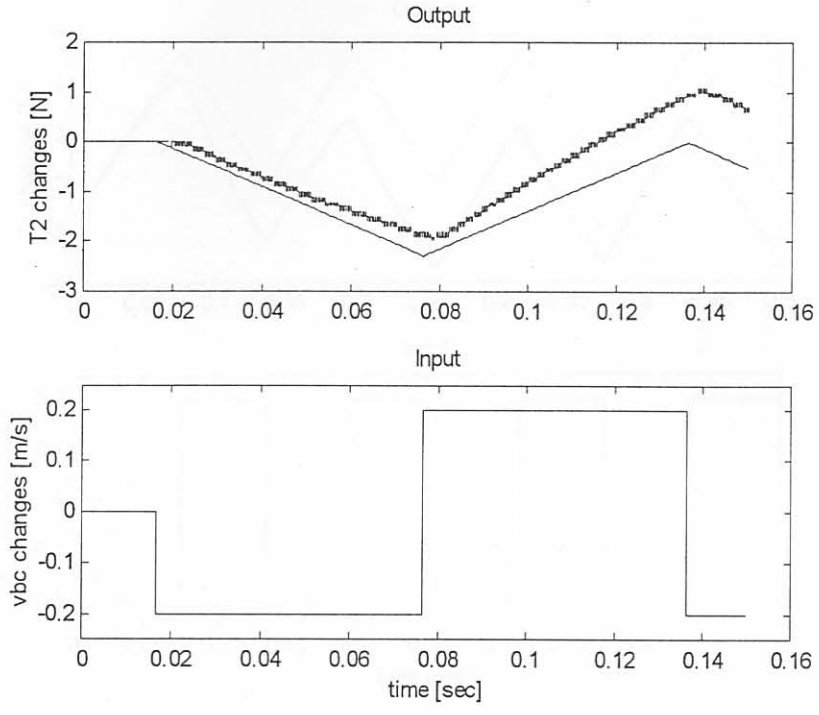

Figure 3.35: I/O data for the identification of $g_{32}(s)$ in the third linear model. (for outputs: upper curve: measured output, lower curve: model output).

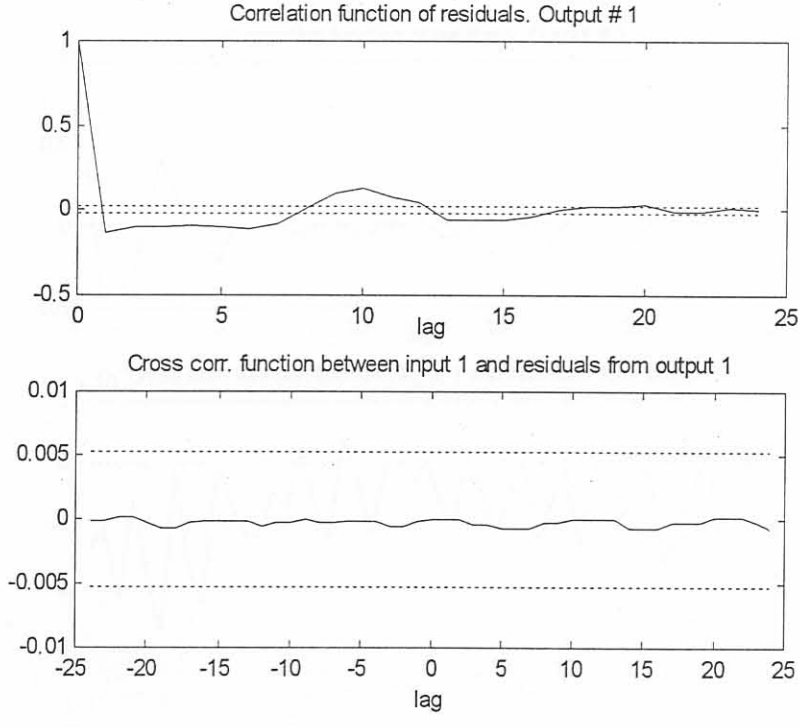

Figure 3.36: Correlation and cross correlation plot of the fitted model for $g_{32}(s)$ in the third linear model. The dotted lines indicate the 99% confidence level.

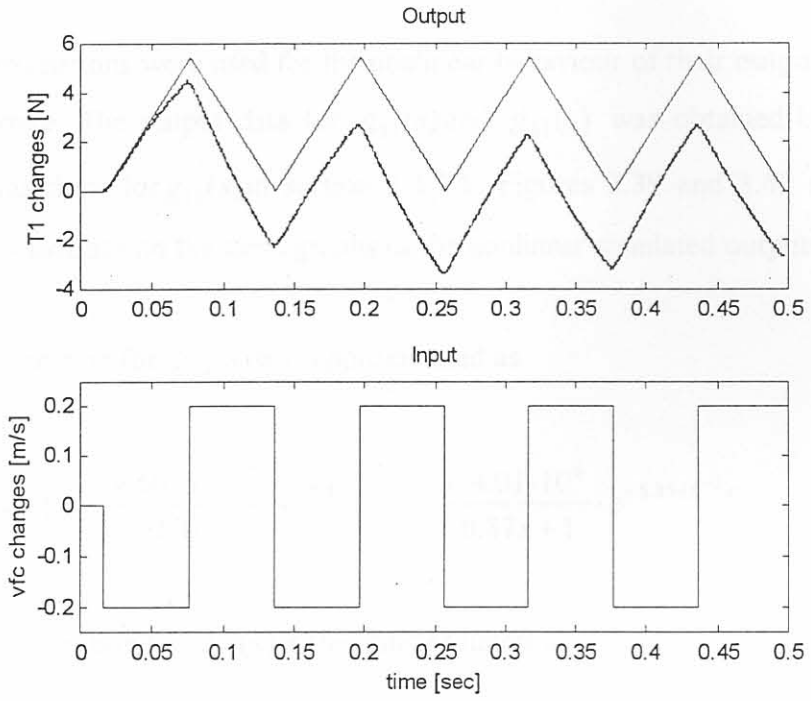

Figure 3.37: I/O data for the identification of $g_{23}(s)$ in the third linear model. (for outputs: upper curve: model output, lower curve: measured output).

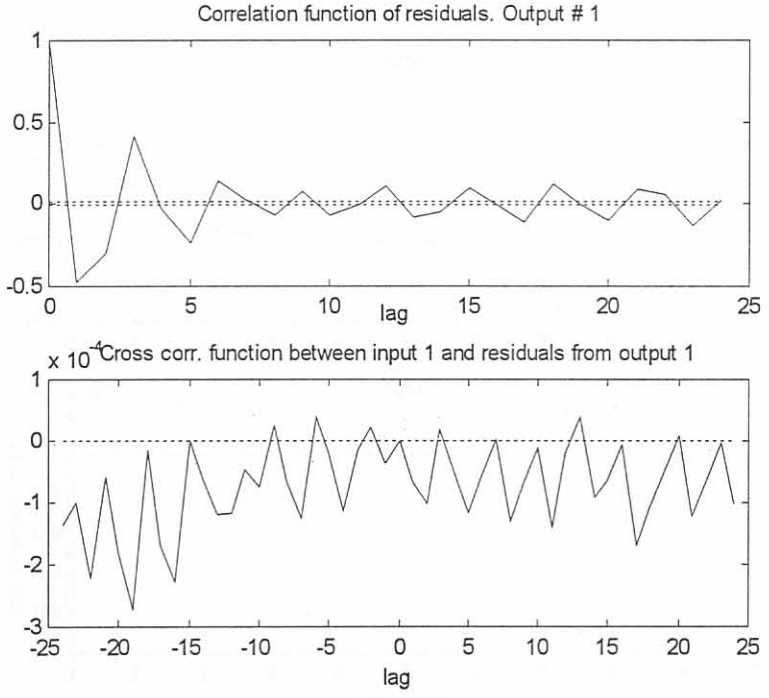

Figure 3.38: Correlation and cross correlation plot of the fitted model for $g_{23}(s)$ in the third linear model. The dotted lines indicate the 99% confidence level.

UNIVERSITEIT VAN PRETORIA
UNIVERSITY OF PRETORIA
YUNIBESITHI YA PRETORIA

3.4.3.4 Transfer Functions $g_{21}(s)$ and $g_{31}(s)$

Linear approximations were used for the nonlinear behaviour of their output responses to a hydraulic stroke. The output data for $g_{21}(s)$ and $g_{31}(s)$ was obtained by a subtraction similar as was done for $g_{11}(s)$ in section 3.4.2.1. Figures 3.39 and 3.40 show the linear model approximations on the same graphs as the nonlinear simulated outputs.

The transfer function for $g_{21}(s)$ was approximated as

$$g_{21}(s) = \frac{-4.6035 \cdot 10^6}{s+1.1481} \cdot e^{-5.85 \cdot 10^{-3} s} = \frac{-4.01 \cdot 10^6}{0.87s+1} \cdot e^{-5.85 \cdot 10^{-3} s} \quad . \tag{3.28}$$

A linear approximation for $g_{31}(s)$ is the transfer function

$$g_{31}(s) = \frac{-1.1928 \cdot 10^6}{s+1.1763} \cdot e^{-5.85 \cdot 10^{-3} s} = \frac{-1.014 \cdot 10^6}{0.85s+1} \cdot e^{-5.85 \cdot 10^{-3} s} \quad . \tag{3.29}$$

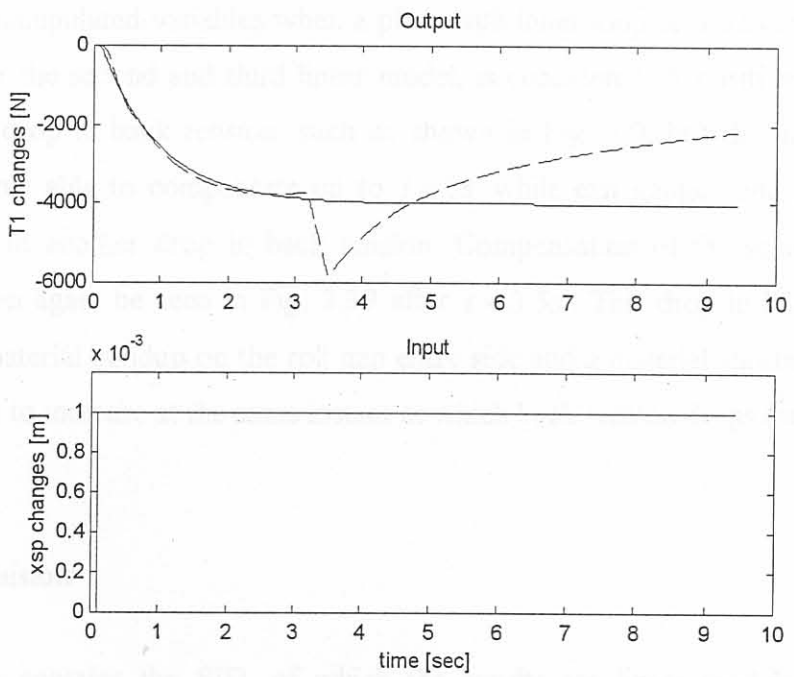

Figure 3.39: I/O data for the identification of $g_{21}(s)$ in the third linear model. (for outputs: solid: model output, dashed: measured output).

UNIVERSITEIT VAN PRETORIA
UNIVERSITY OF PRETORIA
YUNIBESITHI YA PRETORIA

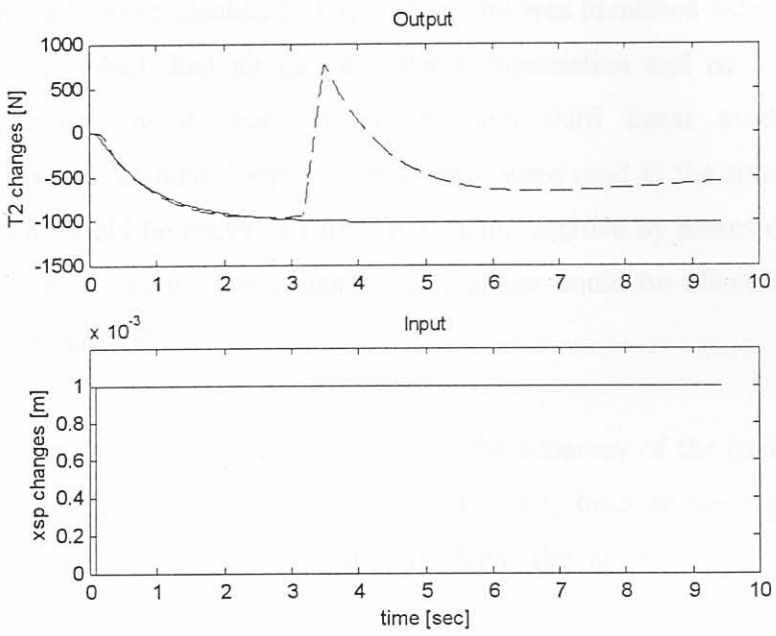

Figure 3.40: I/O data for the identification of $g_{31}(s)$ in the third linear model (for outputs: solid: model output, dashed: measured output).

The nonlinear behaviour of $g_{21}(s)$ and $g_{31}(s)$ can be attributed to a disturbance due to exit gauge/tension interaction since the tensions are the controlled variables and the coiler speeds the manipulated variables when a plant with inner loop tension control, such as the simulator for the second and third linear model, is considered. A positive hydraulic stroke results in a drop in back tension, such as shown in Fig. 3.9, but the inner loop tension control is only able to compensate up to $t \approx 3s$ while exit gauge continues to decrease. This results in another drop in back tension. Compensation of the second back tension drop can then again be seen in Fig. 3.39 after $t \approx 3.5s$. This drop in back tension is the result of a material buildup on the roll gap entry side and a material shortage is causing the front tension to increase at the same instant at which back tension drops (see Fig. 3.40).

3.5 Conclusion

This chapter contains the SID, of which the results are linear models used to design controllers for the nonlinear plant. The data for SID purposes were obtained by running the nonlinear plant simulator at an operating point, at which the mill main drive speed was forced constant, on the speed up ramp of the mill.

UNIVERSITEIT VAN PRETORIA
UNIVERSITY OF PRETORIA
YUNIBESITHI YA PRETORIA

Three linear models were identified. The first model was identified from simulations with a plant simulator, which had no gauge meter compensation and no inner loop tension control incorporated in it. For the second and third linear model gauge meter compensation as well as inner loop tension control were used in the simulator. The result was that tensions could be prevented from becoming negative by means of tension control and the influence of tension variations on exit gauge could be eliminated by means of gauge meter compensation.

With the SID an attempt was made to focus on the accuracy of the transfer functions on the diagonal of the transfer function matrix in Eq. 3.1, because these transfer functions relate the plant outputs to those inputs that have the most direct influence on their corresponding outputs.